Journal of Materials Chemistry A

RSC Publishing

PAPER

View Article Online
View Journal | View Issue

Cite this: J. Mater. Chem. A, 2013, 1, 11894

Niobium pentoxide hollow nanospheres with enhanced visible light photocatalytic activity†

Lihong Li,[a] Jinxia Deng,[a] Ranbo Yu,[a] Jun Chen,[a] Zheng Wang[a] and Xianran Xing*[ab]

Received 3rd July 2013
Accepted 29th July 2013

DOI: 10.1039/c3ta12599h

www.rsc.org/MaterialsA

Herein, we developed a simple template-free synthetic method for producing niobium pentoxide (Nb_2O_5) hollow nanospheres, and fabricated $KNbO_3$ hollow nanospheres which retained the morphology of the template Nb_2O_5 hollow nanospheres by the molten salt method. The formation of Nb_2O_5 hollow nanospheres was *via* Ostwald ripening, and the structural evolution between niobium oxide and niobates was a kind of self-sacrificing templated process. These Nb_2O_5 hollow nanospheres with high surface energy (001) planes showed high thermal stability and large surface area. Furthermore, they not only showed strong intensity of blue emission, but they were also able to efficiently split water under visible light irradiation, and show potential for application as sensors, optoelectronic devices and promising photocatalysts for water splitting under visible light. Due to the high thermal stability of Nb_2O_5 hollow nanospheres and the simplicity of the protocol, we anticipate that this work will enrich the hollow nanostructures of inorganic compounds and provide a new strategy to synthesize hollow nanospheres of niobates and other kinds of materials.

1 Introduction

Nb_2O_5 is one of the most important semiconductor materials, with promising applications in electrochromic materials, field-emission displays, microelectronics, and Li-ion batteries, as well as in catalysis,[1–14] mainly for hydration, dehydration, hydrolysis, condensation, photodegradation of harmful organic contaminants[3] and photolysis of water to produce hydrogen,[4,11] which is environmentally friendly and promising for energy issues. It was reported that Nb_2O_5 had better catalytic activity than TiO_2 and ZnO for indigo carmine degradation after 10 reaction cycles, confirming the easy recovery and long-term stability of Nb_2O_5 in photocatalysis.[3] Recently, Zhang *et al.* reported that carbon modified Nb_2O_5 nanostructures exhibited visible light photocatalytic activity.[4] Unfortunately, the efficiency of the Nb_2O_5 species was not satisfactory, and most other documented photocatalysts based on Nb_2O_5 are only active under ultraviolet light irradiation, which constitutes only a small fraction (<5%) of the solar spectrum. In respect of the efficient utilization of solar energy and indoor artificial illumination, the development of novel Nb_2O_5 photocatalysts with enhanced visible light activity is imperative.

Hollow spheres of metal oxides are exceptionally promising materials in diverse fields of technology, including catalysis,[8] drug and gene delivery,[15] solar cells,[16] photonics and photovoltaics,[17,18] tunable optical properties[19] and rechargeable batteries.[20,21] Specifically, the luminescence properties of some materials could be strongly enhanced by the hollow structure, so it is reasonable to believe that hollow materials with mesoporous structure and high surface area could also make an active contribution to optical properties, such as photolysis. Therefore, hollow nanospheres of Nb_2O_5 have become desirable. Xue *et al.* reported that hollow nanospheres of Nb_2O_5 have been obtained.[22] However, in this method, a large amount of Ti metal was added as a required raw material. Hence a simple and low cost method is needed. The recent upsurge in the reports of novel template-free or self-templated routes for the preparation of hollow particles simultaneously underscores their importance and their facile operation. The utilization of some physical phenomena, such as the Kirkendall effect[23] or Ostwald ripening,[24] provides new opportunities for the template-free fabrication of hollow spheres. Among them, mass transport *via* Ostwald ripening (a spontaneous process involving the growth of large precipitates at the expense of smaller precipitates, caused by energetic factors)[24] has been proven to be a facile approach to generate interior spaces in inorganic nanostructures.[25] In the present work, we introduce a simple template-free synthetic scheme to obtain Nb_2O_5 hollow nanospheres. In addition, Nb_2O_5 is the preferred raw material to form other niobates (such as $ANbO_3$ (A = Li, Na, K, *etc.*) and

[a]Department of Physical Chemistry, University of Science and Technology Beijing, Beijing 100083, China. E-mail: xing@ustb.edu.cn; Fax: +86 6233 2525; Tel: +86 6233 4200

[b]State Key Laboratory for Advanced Metals and Materials, University of Science and Technology Beijing, Beijing 100083, China

† Electronic supplementary information (ESI) available: Synthesis of niobium oxalates; energy-dispersive X-ray (EDX) analysis, XRD pattern, SEM image, TEM image, TG-DSC and FTIR patterns of Nb_2O_5 hollow nanospheres; XRD pattern and TEM image of Nb_2O_5 solid nanospheres. See DOI: 10.1039/c3ta12599h

$M_IM_{II}Nb_3O_{10}$ (M_I = Li, Na, K, Rb, Cs, Tl; M_{II} = Ca)), which have considerable nonlinear optical, ferroelectric, piezoelectric, ionic conductive, pyroelectric, photorefractive, and photocatalytic properties.[26–28] In our previous work, we obtained microscale one and two dimensional niobates with high piezoelectric properties from rodlike and platelet structured Nb_2O_5 *via* a topochemical method based on a molten salt synthesis (MSS).[29,30] The advantages of MSS are its rapid and large-scale fabrication of materials and the control of powder morphology.[31,32] However, it is still a challenge, unlike the microscale, to transform nanoscale Nb_2O_5 hollow spheres to nanoscale alkaline niobate hollow spheres, which are too small to control.

Therefore, not only were the synthesis and properties of Nb_2O_5 hollow nanospheres investigated, but also the transformation between Nb_2O_5 and hollow niobate nanospheres. Herein, we use a simple template-free synthetic scheme to obtain carbon modified Nb_2O_5 hollow nanospheres, and realize control over the solid or hollow interiors of the nanospheres. Significantly, we also demonstrate that the morphology of the template Nb_2O_5 hollow nanospheres can be easily retained by using the molten salt method to prepare $KNbO_3$ hollow nanospheres. To illustrate the satisfactory function of the template and its high thermal stability, the Nb_2O_5 hollow nanospheres were treated at a high temperature of 800 °C for 2 h and 600 °C for 40 h. The structural and morphology evolution were deduced. In addition, the optical properties of the as-prepared Nb_2O_5 hollow nanospheres were studied. These hollow nanospheres showed intense blue emission and were able to efficiently split water under visible light irradiation, exhibiting their potential for use in promising optoelectronic devices and as photocatalysts for water splitting under visible light.

2 Experimental section

2.1 Synthesis

All chemicals were analytical grade reagents, which were bought from Sinopharm Chemical Reagent Beijing Co., Ltd and used without further purification. Preparation of Nb_2O_5 spheres: 500 mg of the as-prepared niobium oxalate, the preparation of which can be found in ESI,† was dissolved in 30 mL of deionized water. The solution was poured into a 50 mL Teflon-lined autoclave and heated for 1–48 h at 220 °C. After the hydrothermal treatment, the fresh precipitates were collected by centrifugation, washed several times with distilled water and absolute ethanol, and finally dried in air at 50 °C. Preparation of Nb_2O_5 hollow spheres: 500 mg of the prepared niobium oxalate and 7.8 mg of $NaH_2PO_4 \cdot 2H_2O$ were dissolved in 30 mL of deionized water. The solution was treated as described above for the preparation of Nb_2O_5 spheres. The as-synthesized Nb_2O_5 hollow spheres were heated at predetermined temperatures of 200, 400, 600, and 800 °C for 2 h, and 600 °C for 40 h. For the synthesis of $KNbO_3$ hollow spheres, the as-prepared Nb_2O_5 hollow spheres were treated at 600 °C for 2 h and then mixed with an equal mole ratio of K_2CO_3, and the mixture was then heated at 770 °C for 10 min in an equal weight of molten KCl salt. The remnant molten salts were removed from the products by washing with hot deionized water several times.

2.2 Characterization

The structure of the samples was characterized by X-ray diffraction (XRD, model M21XVHF22), and the microstructure of the samples was observed using a field-emission scanning electron microscope (FE-SEM, model ZIESS SUPRA 55). The composition of the powders was determined by energy dispersive X-ray (EDX) analysis in the FE-SEM. High-resolution transmission electron microscopy (HRTEM) images were recorded on a JEOL 2010 microscope with an accelerating voltage of 200 kV. Transmission electron microscopy (TEM) observations were performed on a transmission electron microscope (model JEM-100CXII, JEOL, Japan). Raman scattering data were collected in the frequency range of 100–1100 cm^{-1} using a Raman spectrometer (model JYT6400, Jobin Yvon, France). The luminescence spectra of the samples were recorded in cuvettes (1 cm path length) on an F-4500 FL Spectrophotometer at room temperature. Nitrogen physisorption experiments were carried out using a Quantachrome Autosorb-1 analyser at −196 °C. Before the measurement, degassing was conducted at 100 °C for 6 h to remove possible moisture.

2.3 Photocatalytic measurements

The activities of the as-prepared catalysts, compared with commercial Nb_2O_5, for photocatalytic hydrogen production were carried out in an outer irradiation quartz cell, which was connected to a closed gas circulation system. 50 mg of the photocatalyst loaded with 3 wt% Pt was dispersed in a Na_2SO_3 aqueous solution (100 mL of distilled H_2O, 2.5 g of Na_2SO_3), and then visible light ($\lambda > 420$ nm) from a 300 W xenon arc lamp was irradiated through a long-pass cutoff filter (Changtuo, China). The evolved H_2 was determined with a gas chromatograph (Beijing, GC-3240, TCD, Ar carrier), which was connected to a gas circulating line.

3 Results and discussion

Nb_2O_5 hollow nanospheres were prepared by the hydrothermal treatment of mixtures of niobium oxalates and $NaH_2PO_4 \cdot 2H_2O$ at 220 °C for 48 h (marked as NBHS-48). The as-synthesized sample consists of a high yield of Nb_2O_5 spheroids with an average diameter of 300 nm (Fig. 1a). The high-magnification image clearly shows that the individual nanospheres are hollow (see the inset of Fig. 1a). Energy-dispersive X-ray (EDX) analysis (see Fig. S1†) of the hollow spheres confirms that the ratio of Nb : O is very nearly 2.0 : 5.0. The phase purity of the products was examined by X-ray diffraction (Fig. S2a†). It is interesting to find that only two peaks at around 23° and 46° can be observed from the XRD pattern. By careful analysis, both of the peaks can be assigned to the {001} plane reflection of the orthorhombic phase of Nb_2O_5 (JCPDS 30-873), which indicates that the surface planes of the product are aligned unidirectionally, normal to the (00*l*) face. Fig. 1b and c show the TEM and HRTEM images of the typical hollow spheres,

which reveal that the shell of a single hollow nanosphere is composed of rodlike nanoparticles 5–10 nm in width. The clear lattice image demonstrates that the nanorods are single-crystalline in nature, and the distance between neighboring lattice-fringes was measured to be 0.390 nm, close to that of the (001) lattice spacing (0.393 nm) in the orthorhombic phase of T-Nb_2O_5 (space group *Pbam*). This indicates that the small rods of the shell point out of the hollow sphere along the [001] direction. For comparison, the typical Nb_2O_5 solid spheres were obtained without $NaH_2PO_4 \cdot 2H_2O$ (see Fig. 1), treated at 220 °C for 8 h and 48 h, respectively. From the FE-SEM and TEM images (Fig. 1d and S3a†), the product treated for 8 h consists of solid spheres with diameters of 200–500 nm with small needles on the surface of the spheres. Extending the reaction time to 48 h resulted in the large growth of the needles (Fig. 1e). The XRD profile (Fig. S3b†) indicates that the crystallographic phase of the spheres prepared by hydrothermal treatment for 48 h is that of orthorhombic Nb_2O_5 (JCPDS 30-873).

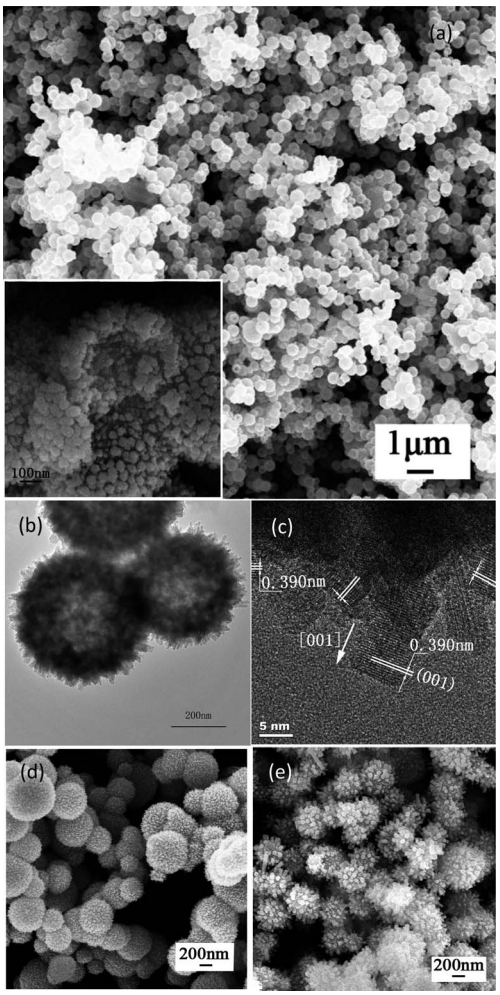

Fig. 1 (a) SEM image of NBHS-48 (inset: high-magnification images) (b) TEM image and (c) HRTEM image of Nb_2O_5 hollow nanospheres; of the corresponding Nb_2O_5 hollow nanosphere. (d) and (e) FE-SEM images of the as-synthesized Nb_2O_5 solid spheres synthesized by the hydrothermal treatment at 220 °C for 8 h and 48 h, respectively.

To obtain a complete view of the formation process of the hollow nanospheres and their growth mechanism, a detailed time-dependent morphology evolution study was conducted by TEM and SEM measurements (Fig. 2a–h). With a short reaction time (2 h, Fig. 2a and e), the sample contains spherical colloidal aggregates with an average diameter of 120 nm. Upon prolonging the reaction aging time to 8 h (Fig. 2b and f) and 24 h (Fig. 2c and g), it is obvious to see that the nanospheres undergo a hollowing process. At a reaction time of 48 h (Fig. 2d and h), the formed hollow nanospheres are uniform with a 100% morphological yield. It is also found that during the hollowing process, the size of these nanospheres does not change much. This observation illustrates that the hollowing process is essentially similar to that observed previously in the preparation of pure anatase TiO_2 hollow spheres.[33]

To study the thermal and chemical stabilities, the NBHS-48 were treated at 200, 400, 600, and 800 °C for 2 h (labelled as NBHS-200, NBHS-400, NBHS-600, and NBHS-800), and 600 °C for 40 h (labelled as NBHS-600-40), respectively. The XRD patterns of these samples are similar to that of NBHS-48 (Fig. S2†), which indicates that their phases do not change much. Meanwhile, from the TEM image (Fig. S4†), no corrupt hollow nanospheres could be observed and the morphology of the Nb_2O_5 particles is maintained, which indicates the high thermal stability of the Nb_2O_5 hollow nanospheres.

To determine the detailed structure of the Nb_2O_5 hollow nanospheres, TG-DSC measurements (Fig. S5†) and FTIR spectra (Fig. S6†) were recorded for the sample NBHS-48. From the TG pattern, at around 100 °C the weight reduced by about 0.5%, and from 200 °C to 400 °C the weight further reduced by about 1.5%, which might correspond to the escape of the adsorbed water and carbon that might be formed from oxalates absorbed over the surface of the product, respectively. From the DSC curve, the typical peaks could be observed above 800 °C which indicated that the T-type Nb_2O_5 transformed into H-type Nb_2O_5, which was in agreement with the results reported in ref. 34. FTIR analysis confirmed the formation of carbon modified Nb_2O_5. The stretching vibration of the C–O in the Nb–O–C structure results in two peaks at 1080 and 1042 cm^{-1}, similar to those of Ti–O–C, which suggested that the carbon exists in the form of carbonate species in NBHS-48. From the Raman spectra (Fig. 3) of NBHS-48, NBHS-200, NBHS-400, NBHS-600, and NBHS-800, it was found that they were quite similar to each other. With the increase of sintering temperature (from room temperature to 400 °C), the corresponding slight shifts of the Raman bands from 230 cm^{-1} to 234 cm^{-1} and 705 cm^{-1} to 710 cm^{-1} might be also caused by the absorbed water, carbon, and the increasing bond order of the niobia polyhedra and the Nb–O–Nb linkages; with further increase of temperature above 400 °C, no shift of the Raman bands was observed, which was in agreement with those of the T-Nb_2O_5 reported in the literature.[35]

Furthermore, due to the high thermal and chemical stabilities of the as-prepared Nb_2O_5 hollow nanospheres, we attempted to use them as templates to synthesize hollow niobate nanospheres. Pure $KNbO_3$ (a favorable piezoelectric material) hollow nanospheres, which could be assigned to the

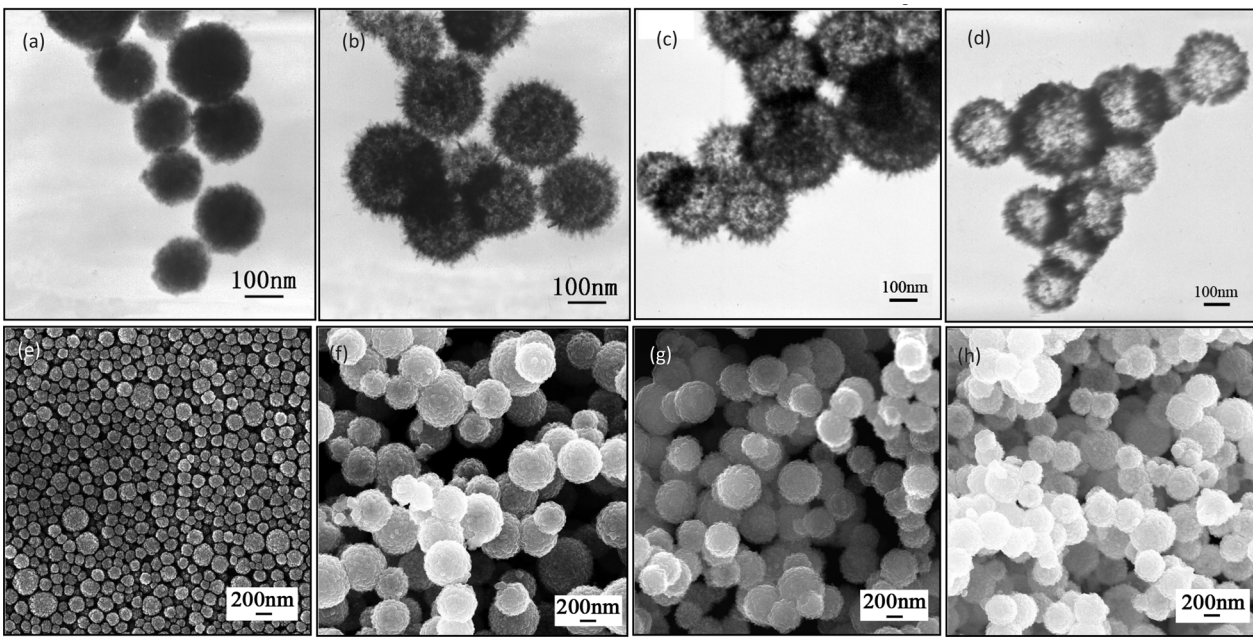

Fig. 2 Morphology evolution of the Nb_2O_5 hollow nanospheres with reaction time: TEM images of the products obtained at 220 °C after (a) 2 h, (b) 8 h, (c) 24 h, and (d) 48 h, and the corresponding SEM images of the products obtained at 220 °C after (e) 2 h, (f) 8 h, (g) 24 h, and (h) 48 h, respectively.

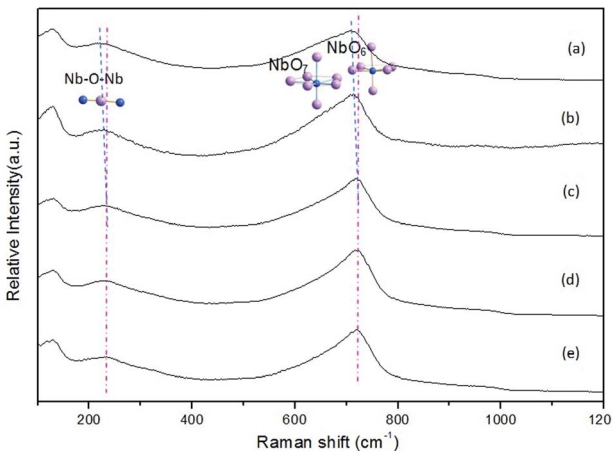

Fig. 3 Raman spectra of NBHS-48, NBHS-200, NBHS-400, NBHS-600 and NBHS-800.

rhombohedral phase (JCPDS 71-947) with lattice parameters of $a = 4.016$ Å and $\alpha = 89.817°$ (see Fig. 4a) were successfully obtained by the molten salt method at 770 °C for a short time. From the SEM and TEM images (Fig. 4b and S7†), although the particles making up the shells changed from rods to cubes, the $KNbO_3$ hollow nanospheres still retained the morphology of the precursor Nb_2O_5 hollow nanospheres.

Based on the above experimental results, possible mechanisms of formation and morphology evolution were proposed. As illustrated in Fig. 5, during the hydrolysis reactions, both the solid spheres and hollow nanospheres firstly went through an aggregation stage, and then underwent either crystal growth or Ostwald ripening at the subsequent stage, respectively. If there was no phosphate in the system, the crystal growth processing occurred. The small protuberances on the surfaces of the solid spheres, which provided many high-energy sites for crystal growth, grew up along the 1D direction. If the phosphate was added to the system, Ostwald ripening occurred. The presence of the phosphate was the crucial factor that induced the formation of the hollow structure of Nb_2O_5. Firstly, the phosphates over the surface of the hollow nanospheres served as a diffusion boundary to restrain rapid crystal growth, and prevented direct fusion of the nanospheres during the ripening. Secondly, the phosphate ions had a coordination effect with the Nb^{5+} ions. As the inner crystallites of the Nb_2O_5 spheres would dissolve, the following reactions might take place:

$$Nb(HC_2O_4)_5 \cdot 6H_2O + 5NaH_2PO_4 \cdot 12H_2O \rightarrow Nb(OH)_5 + 5NaHC_2O_4 + 5H_3PO_4 + 61H_2O \quad (1)$$

$$Nb(OH)_5 + xPO_4^{3-} \rightarrow [Nb(PO_4)_x]^{5-3x} + 5OH^- \quad (2)$$

The formation of $[Nb(PO_4)_x]^{5-3x}$ drives eqn (1) toward the right-hand side and speeds up the dissolution of the high-surface energy inner crystallites of the spheres, producing channels connecting the inner space and the outer space in the oxide shells. Due to the two effects of the phosphate ions, the presence of phosphate ions plays a key role in whether the Ostwald ripening occurs or not.

From the structure of T-Nb_2O_5,[34] the intrinsic formation of the nanorods that composed the shell of the hollow nanospheres was further revealed. Edge-sharing NbO_6 and NbO_7 units are parallel to the *ab* plane, which have higher surface energy than that of the plane with corner-sharing units (Fig. 5).

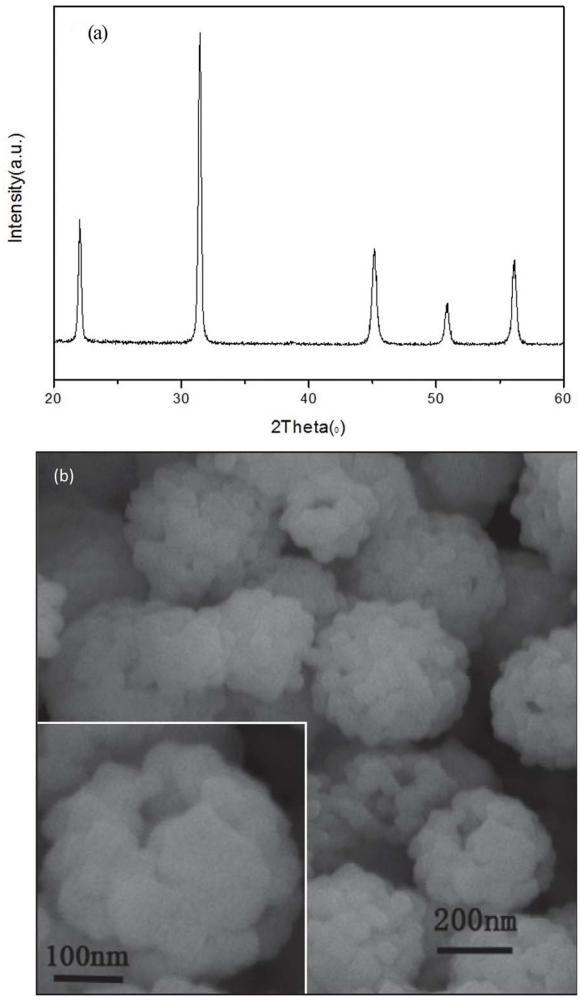

Fig. 4 (a) XRD pattern and (b) SEM image of $KNbO_3$ (inset: high-magnification images).

Therefore, on the one hand, to reduce the total surface energy the nanoparticles were then oriented along the (001) plane with high surface energy; on the other hand, due to the formation process of the hollow spheres, the small rods did not grow and the (001) plane was still the dominant plane.

The transformation process from Nb_2O_5 hollow nanospheres to perovskite $KNbO_3$ hollow nanospheres was a kind of self-sacrificing templated process. In the molten salt, K^+ needed to diffuse inside T-Nb_2O_5, and this process involved bond breaking, rebonding, and generation of new bonds. Viewed along the *c* axis of Nb_2O_5, NbO_6 and NbO_7 units are corner-sharing, and in the perovskite $KNbO_3$ crystal, NbO_6 octahedron units are connected by sharing corners along the *a*, *b*, and *c* axes. Therefore, although the small rods of the shell became cubes, due to the high thermal stability of the Nb_2O_5 hollow nanospheres and the similarity of the structures of Nb_2O_5 and $KNbO_3$, the morphology of the hollow spheres could be maintained, and $KNbO_3$ hollow nanospheres were obtained. It is reasonable to conclude that the molten salt method is a facile and fast strategy to synthesize hollow nanospheres of niobate and other kinds of materials.

The luminescence characteristics of the hollow nanospheres NBHS-200 and commercial Nb_2O_5 with different morphologies were investigated at room temperature, as shown in Fig. 6a (λ_{ex} = 382 nm). Comparing the spectra of the two kinds of Nb_2O_5, both of them present blue emission bands at 440–480 nm, and the Nb_2O_5 hollow nanospheres exhibit a much stronger typical blue emission peak at about 450 nm. Hollow crystals are expected to exhibit high light-collection efficiency and enhanced luminescence performance due to their hollow structures and large internal surface area.[36] Moreover, the carbonate species on the surface may also affect the luminescence characteristics.

To further study the photocatalytic properties of the Nb_2O_5 hollow nanospheres, photocatalytic H_2 evolution under visible light irradiation from an aqueous solution containing the sacrificial reagent anhydrous sodium sulfite was utilized to investigate the photocatalytic activities of the materials treated at different temperatures with Pt (3 wt%) loading (Fig. 6b). The rates of H_2 production of NBHS-48, NBHS-200, and NBHS-400 were 25, 130 and 40 μmol h^{-1} g^{-1}, respectively, and no H_2 was evolved from commercial Nb_2O_5. It could be observed that the NBHS-200 sample exhibited promising photocatalytic activity, and it was the best visible-light responsive photocatalyst among these Nb_2O_5 samples, the rate of H_2 production of which was almost 19 times that (7 μmol h^{-1} g^{-1}) reported in ref. 4. The surface areas of NBHS-48, NBHS-200 and NBHS-400 were investigated using the nitrogen adsorption–desorption isotherm (Fig. 7). The isotherms were identified as type IV,[37] which is characteristic of mesoporous materials, and their Brunauer–Emmett–Teller (BET) specific surface areas are large (132 m^2 g^{-1}, 167 m^2 g^{-1} and 166 m^2 g^{-1}, respectively). In general, the photocatalytic properties of oxides strongly depend on their structure and surface properties, including surface area and adsorption. The enhanced visible light photocatalytic activity of NBHS-200 should be first attributed to its greater visible light absorption because of the modification with carbonate species, which was different to that of NBHS-48, and the lower photocatalytic properties of NBHS-400 might be caused by the reduced amount of carbonate species on its surface. The high surface energy (001) plane, large surface area and mesoporous structure could also contribute to the splitting water property. In this sense, the as-prepared carbon-modified Nb_2O_5 hollow nanospheres are exciting and may have significant technological applications as sensors, optoelectronic devices and catalysts.

4 Conclusions

In summary, we developed a simple template-free synthetic method for producing Nb_2O_5 hollow nanospheres, and fabricated $KNbO_3$ hollow nanospheres. Niobium pentoxide (Nb_2O_5) hollow nanospheres with high surface energy (001) planes were synthesized by a hydrothermal method with the addition of $NaH_2PO_4 \cdot 2H_2O$ *via* Ostwald ripening. The morphology of the template Nb_2O_5 hollow nanospheres could be retained by the molten salt method to prepare $KNbO_3$

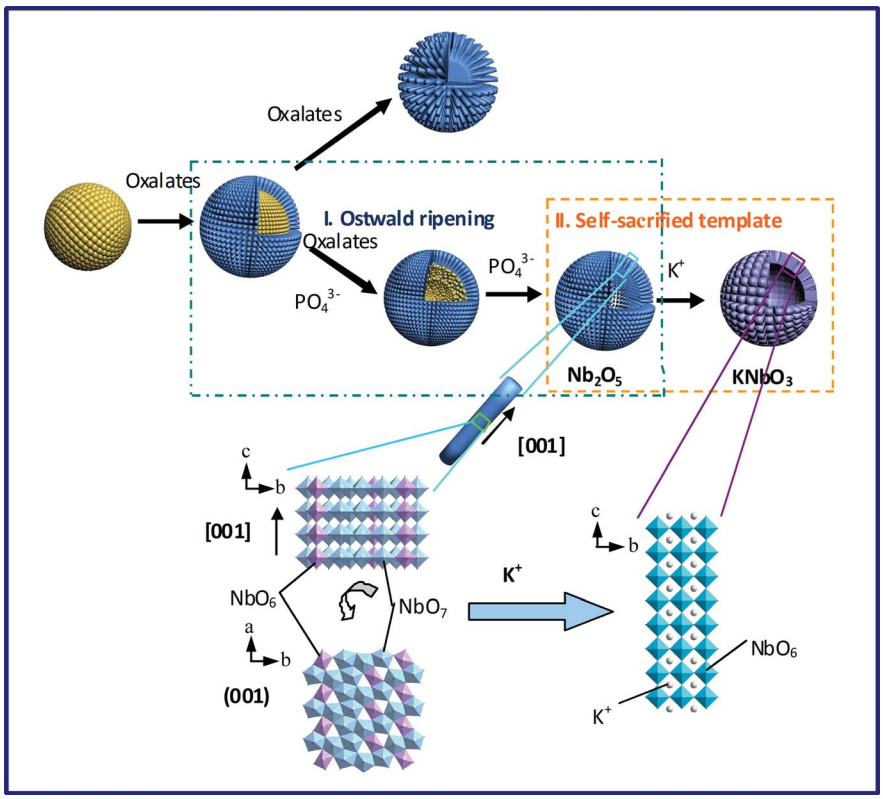

Fig. 5 Formation processes and structure evolution of hollow spheres and solid spheres.

hollow nanospheres. The as-prepared Nb_2O_5 hollow nanospheres showed intense blue emission and were able to efficiently split water under visible light irradiation, demonstrating their potential as promising materials for optoelectronic devices and photocatalysts for water splitting under visible light, which would have potential for application in sensors and optoelectronic devices. Due to the high thermal stability of Nb_2O_5 hollow nanospheres and the simplicity of the protocol, we anticipate that this work will enrich the hollow nanostructures of inorganic compounds and provide a new strategy to synthesize hollow nanospheres of niobate and other kinds of materials.

Acknowledgements

This work was financially supported by the National Natural Science Foundation of China (Grant Nos. 21231001, 20921001, 21301180 and 21131004). The authors thank Prof. Yadong Li for the helpful discussions on this study.

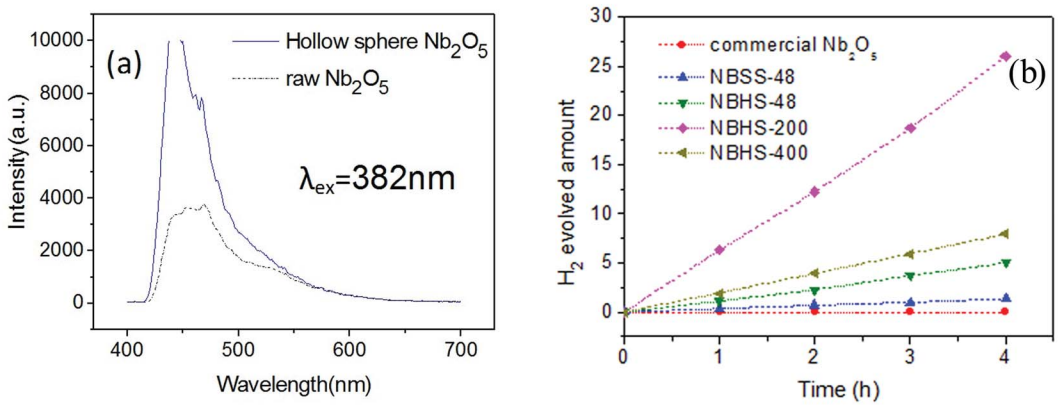

Fig. 6 (a) Emission spectra of the products with different structures at room temperature. (b) The amount of hydrogen evolved after 4 h of irradiation for visible light photocatalysis using different catalysts (50 mg of which loaded with 3 wt% Pt was dispersed in a Na_2SO_3 aqueous solution (100 mL of distilled H_2O, 2.5 g of Na_2SO_3)).

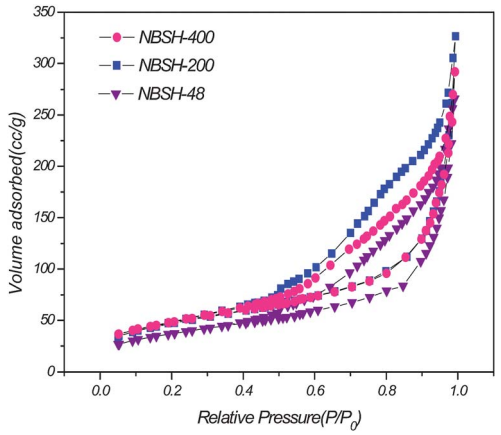

Fig. 7 N_2 adsorption–desorption isotherms of NBSH-48, NBSH-200 and NBSH-400.

Notes and references

1 P. Carniti, A. Gervasini, S. Biella and A. Auroux, *Catal. Today*, 2006, **118**, 373–378.
2 B. V. R. Chowdari, A. Le Viet, M. V. Reddy, R. Jose and S. Ramakrishna, *J. Phys. Chem. C*, 2010, **114**, 664–671.
3 J. B. de Paiva, Jr, W. R. Monteiro, M. A. Zacharias, J. A. J. Rodrigues and G. G. Cortez, *Braz. J. Chem. Eng.*, 2006, **23**, 517–524.
4 S. X. Ge, H. M. Jia, H. X. Zhao, Z. Zheng and L. Z. Zhang, *J. Mater. Chem.*, 2010, **20**, 3052–3058.
5 Y. Li, S. Yan, L. Qian, W. Yang, Z. Xie, Q. Chen, B. Yue and H. He, *J. Catal.*, 2006, **241**, 173–179.
6 M. Mozetič, U. Cvelbar, M. K. Sunkara and S. Vaddiraju, *Adv. Mater.*, 2005, **17**, 2138–2142.
7 T. Okuhara, M. Kimura, T. Kawai, Z. Xu and T. Nakato, *Catal. Today*, 1998, **45**, 73–77.
8 M. C. Orilall, N. M. Abrams, J. Lee, F. J. DiSalvo and U. Wiesner, *J. Am. Chem. Soc.*, 2008, **130**, 8882–8883.
9 N. Özer, D. G. Chen and C. M. Lampert, *Thin Solid Films*, 1996, **277**, 162–168.
10 M. Paulis, M. Martín, D. B. Soria, A. Díaz, J. A. Odriozola and M. Montes, *Appl. Catal., A*, 1999, **180**, 411–420.
11 A. G. S. Prado, L. B. Bolzon, C. P. Pedroso, A. O. Moura and L. L. Costa, *Appl. Catal., B*, 2008, **82**, 219–224.
12 M. Zumer, V. Nemanic, B. Zajec, M. Remskar, A. Mrzel and D. Mihailovic, *Appl. Phys. Lett.*, 2004, **84**, 3615–3617.
13 M. Habibi and R. Mokhtari, *J. Inorg. Organomet. Polym. Mater.*, 2012, **22**, 158–165.
14 Y. Zhao, C. Eley, J. Hu, J. S. Foord, L. Ye, H. He and S. C. E. Tsang, *Angew. Chem., Int. Ed.*, 2012, **51**, 3846–3849.
15 M. Ferrari, *Nat. Rev. Cancer*, 2005, **5**, 161–171.
16 Z. Dong, X. Lai, J. E. Halpert, N. Yang, L. Yi, J. Zhai, D. Wang, Z. Tang and L. Jiang, *Adv. Mater.*, 2012, **24**, 1046–1049.
17 L. Lu, R. Capek, A. Kornowski, N. Gaponik and A. Eychmüller, *Angew. Chem., Int. Ed.*, 2005, **44**, 5997–6001.
18 H. Du, L. Jiao, Q. Wang, J. Yang, L. Guo, Y. Si, Y. Wang and H. Yuan, *Nano Res.*, 2012, 1–12.
19 G. Duan, W. Cai, Y. Luo and F. Sun, *Adv. Funct. Mater.*, 2007, **17**, 644–650.
20 Z. Wang, L. Wu, M. Chen and S. Zhou, *J. Am. Chem. Soc.*, 2009, **131**, 11276–11277.
21 J. Wang, N. Yang, H. Tang, Z. Dong, Q. Jin, M. Yang, D. Kisailus, H. Zhao, Z. Tang and D. Wang, *Angew. Chem.*, 2013, **125**, 6545–6548.
22 F. Liu and D. F. Xue, *Mod. Phys. Lett. B*, 2009, **23**, 3769–3775.
23 Y. Sun and Y. Xia, *Science*, 2002, **298**, 2176–2179.
24 W. Ostwald, *Z. Phys. Chem.*, 1897, **22**, 289–330.
25 X. B. Cao, L. Gu, L. J. Zhuge, W. J. Gao, W. C. Wang and S. F. Wu, *Adv. Funct. Mater.*, 2006, **16**, 896–902.
26 L. Li, J. Deng, J. Chen, R. Yu, L. Qiao and X. Xing, *J. Alloys Compd.*, 2009, **471**, 428–431.
27 C. Sun, X. Xing, J. Chen, J. Deng, L. Li, R. Yu, L. Qiao and G. Liu, *Eur. J. Inorg. Chem.*, 2007, 1884–1888.
28 X. Sun, J. Deng, J. Chen, C. Sun and X. Xing, *J. Am. Ceram. Soc.*, 2009, **92**, 3033–3036.
29 L. Li, J. Deng, J. Chen, X. Sun, R. Yu, G. Liu and X. Xing, *Chem. Mater.*, 2009, **21**, 1207–1213.
30 L. Li, J. Deng, R. Yu, J. Chen, X. Wang and X. Xing, *Inorg. Chem.*, 2010, **49**, 1397–1403.
31 J. Chen, X. Xing, A. Watson, W. Wang, R. Yu, J. Deng, L. Yan, C. Sun and X. Chen, *Chem. Mater.*, 2007, **19**, 3598–3600.
32 L. Li, J. Chen, J. Deng, R. Yu, L. Qiao, G. Liu and X. Xing, *Eur. J. Inorg. Chem.*, 2008, 2186–2190.
33 X. W. Lou, L. A. Archer and Z. Yang, *Adv. Mater.*, 2008, **20**, 3987–4019.
34 G. Blasse and G. P. M. van den Heuvel, *Mater. Res. Bull.*, 1972, **7**, 1041–1043.
35 J.-M. Jehng and I. E. Wachs, *Catal. Today*, 1990, **8**, 37–55.
36 L. Gou and C. J. Murphy, *Nano Lett.*, 2003, **3**, 231–234.
37 A. Vinu, D. P. Sawant, K. Ariga, M. Hartmann and S. B. Halligudi, *Microporous Mesoporous Mater.*, 2005, **80**, 195–203.